JOURNAL OF MATERIALS SCIENCE 35 (2000) 4347–4355

The effects of various hydrothermal treatments on magnesium-aluminium hydrotalcites

L. HICKEY*, J. T. KLOPROGGE, R. L. FROST
Centre for Instrumental and developmental Chemistry, Queensland University of Technology, GPO Box 2434, Brisbane Q 4001, Australia
E-mail: la.hickey@student.qut.edu.au

Mg/Al hydrotalcites were synthesised by coprecipitation followed by hydrothermal treatment. The materials were characterised by XRD, infrared and Raman spectroscopy, electron microscopy and thermal analysis. The XRD pattern obtained was typical of a hydrotalcite, where the interlayer anion is CO_3^{2-}, with a basal distance of ~23.5 Å. All possible CO_3^{2-} modes were observed in the infrared and Raman spectra, at 1068 cm^{-1}, 844 cm^{-1}, ~1380 cm^{-1}, and ~680 cm^{-1}. XRD, Infrared and Raman spectroscopy complimented each other by showing that with treatment the degree of order increased regardless of the type of treatment. Furthermore, it was shown that aging at increased temperature and pressure increased crystallinity and that treatment in water rather than in the mother liquid resulted in a more crystalline material. TEM showed that crystal size increased with aging, such that growth occurred on the edges resulting in the formation of hexagonal plate shaped hydrotalcite crystals. Thermal analysis showed 3 major weight losses corresponding to the loss of interparticle water, interlayer water, and dehydroxylation of the hydroxide layers and decarbonation of the interlayer region.

1. Introduction

Clays are an important group of minerals that are heavily relied on by industry. They are commonly found in nature and can be used to produce a range of versatile materials. The term "clay" encompasses two broad groups: cationic clays that are wide spread in nature, such as smectites, and anionic clays which are rarer in nature but relatively simple and inexpensive to synthesise [1]. Cationic clays consist of negatively charged alumino-silicate layers with cations in the interlayer space to balance the charge [1]. Anionic clays, also known as layered double hydroxides (LDH), possess a structure electrically opposite to that exhibited by cationic clays. Anionic clays further differ from cationic clays in their particle size, such that anionic clays are generally much larger. The most common type of LDH is the hydrotalcite-type (HT) group of minerals, which have a general formula:

$$\left[M^{2+}_{1-x}M^{3+}_{x}(OH)_2\right]^{b+}\left[A^{n-}_{b/n}\right]\cdot mH_2O,$$

where M^{2+} and M^{3+} are the divalent and trivalent cation in the octahedral positions within the hydroxide layers with x normally between 0.17 and 0.33. A^{n-} is an interlayer anion with a negative charge n, b is the charge of the layer and m is the number of water molecules.

The hydrotalcite-type anionic clays have a structure similar to that of brucite, $Mg(OH)_2$, where each Mg^{2+} ion is octahedrally surrounded by six OH^- ions (Fig. 1a). The hydrotalcite structure is obtained when some of the Mg^{2+} ions, in the brucite layer, are replaced by trivalent cations with a similar radius (Fig. 1b) [2]. The higher charge of the cation imposes an overall positive charge in the brucite-type layer. These layers are maintained electrically neutral by the interlayer anions (Fig. 2). There is essentially no limitation on the nature of the anion provided it doesn't form a complex with the cations [1]. The wide range of synthetic materials of this type appeases an extensive range of properties. The application, of the LDH materials depend on the nature of the cation, existing in the brucite–type layers, others depend on the nature of the interlayer anion, and in some cases the material is partially or totally decomposed to yield new ones with specific properties [3]. These applications include for example catalysts and catalyst precursors, ion exchangers and adsorbers, anion scavengers and stabilisers, etc [1, 2, 4–6]. Therefore, studies of the crystal chemistry of hydrotalcite-like compounds have mainly focussed on the influence of their composition on lattice parameters and on physical properties [7].

Although generally anion clay particles are larger than their counterparts, the cationic clays, there is still profuse interest in the ability to increase particle size. Larger crystals are better for characterisation as they contain more interpretable information. Under

* Author to whom all correspondence should be addressed.

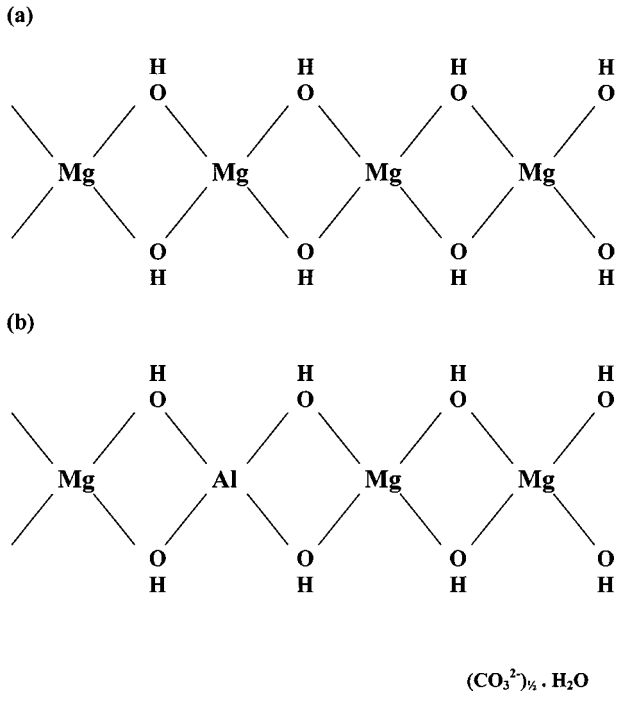

Figure 1 Two-dimensional representation of the structure of the hydroxide layers in: (a) brucite–$Mg(OH)_2$; (b) hydrotalcite–$Mg_6Al_2(OH)_{16}(CO_3^{2-}) \cdot 4H_2O$.

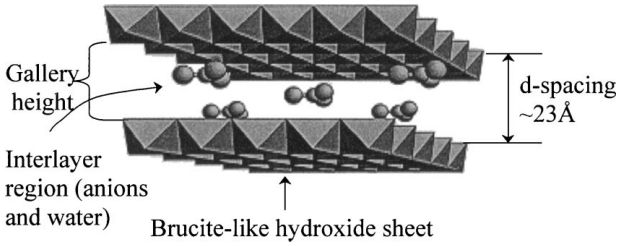

Figure 2 Schematic representation of the hydrotalcite-type anionic clay structure.

laboratory conditions it is difficult, almost impossible, to synthesise so called "giant crystals" [8], however crystals of considerable size have been created. Bigger crystals, eg. zeolites, have been produced by slowly cooling and by applying a temperature gradient to allow the rate of growth to be controlled [8].

Hydrothermal treatment generally increases crystallinity, depending mainly on the temperature although pressure and time also are important parameters. Miyata found, by hydrothermally treating a Mg/Al hydrotalcite, that the temperature of treatment had a dramatic effect on crystallite size, such that size increased up to 180°C but decreased above 200°C [9]. A more recent study investigated the effect of varying time but maintaining a constant temperature [3]. This study found by X-ray diffraction and infrared spectroscopy that the order in the interlayer region and the crystallinity in the hydroxide layer increased with time. Furthermore by using transmission electron microscopy, it was shown that the average size of the lamellar hexagonal particles increased with time [3].

The aim of the present work is to obtain insight into the nature of hydrotalcite-type materials when the experimental conditions during hydrothermal treatment are varied. Samples were treated as a suspension in their own mother liquid or in water, either in a hydrothermal reactor under autogenous water vapour pressure, or in a water bath at 1atm. A comparison of the untreated and treated samples was expected to show different degrees of crystallinity and particle sizes.

2. Experimental

2.1. Preparation

Hydrotalcites with a composition of $Mg_6Al_2(OH)_{16}(CO_3) \cdot 4H_2O$ were synthesised by the coprecipitation method [10–12]. Two solutions were prepared, solution 1 contained 2 M NaOH and 0.125 M Na_2CO_3, solution 2 contained 0.75 M Mg^{2+} [$Mg(NO_3)_2 \cdot 6H_2O$] along with 0.25 M Al^{3+} [$Al(NO_3)_3 \cdot 9H_2O$]. Solution 2 was added to solution 1, using a peristaltic pump at a rate of 40 ml/min, under vigorous stirring while maintaining pH 10. When the addition was complete, the mixture was stirred for a further 1.5 hours, during which time the pH was still maintained at 10. The suspension was then divided into 5 equal portions to undergo different hydrothermal treatments. Two portions, sample 1A and 1B, were not washed and remained in their mother liquid. The remaining portions, samples 2A, 2B and 2C, were thoroughly washed in deionised water. Sample 2A was then dried and underwent no hydrothermal treatment; samples 2B and 2C were resuspended in water before hydrothermal treatment. Sample 1A was placed in a hot water bath at 70°C for 7 days. Sample 1B and 2B were subjected to hydrothermal treatment at autogenous water vapour pressure at 150°C, and at 70°C for sample 2C in teflon lined stainless steel Parr Bombs for 7 days. After aging all hydrothermal samples were washed in deionised water and oven dried at 60°C for 1 hr.

2.2. Characterisation

2.2.1. Powder X-ray diffraction

Powder XRD (XRD) diagrams were recorded on a Phillips wide angle PW 1050/25 vertical goniometer equipped with a graphic diffracted beam monochromator. The *d*-values and intensity measurements were improved by application of an in-house developed computer aided divergence slit system enabling constant sampling area irradiation (20 mm long) at any angle of incidence. The radiation applied was Cu-K_α from a long fine-focus Cu tube operating at 35 kV and 40 mA. The samples were measured in the stepscan mode from 2 to 75°2θ with steps of 0.02°2θ and a counting time of 2 seconds. Jade software package (Materials Data, Inc.) was used to analyse the data, identification of the existing crystalline phases being concluded from the comparison with pre-existing JCPDS diffraction data files. Spectra manipulation and interpretation was performed using TracesV4 (Diffraction Technology Pty. Ltd.) and Microsoft EXCEL.

2.2.2. Thermal analysis

Differential thermal analysis (DTA) and Thermal gravimetric analysis (TG) of the samples were recorded on

a Setaram 2000 (1992) unit. The data were recorded from 30°C to 500°C at heating rate of 2° per minute. Data manipulation and interpretation was carried out using Microsoft EXCEL.

2.2.3. Fourier transform infrared and Raman spectroscopy

Fourier-transform infrared (FTIR) spectra were recorded using the KBr technique (2 wt% sample) on a Perkin Elmer FT-IR 1000 spectrometer; 64 scans were taken to improve the signal to noise ratio in the range of 400–4000 cm^{-1}, the normal resolution was 4 cm^{-1}. The Raman spectra were obtained using a Renishaw 1000 Raman Microscope System, which includes a monochromator, a filter system and a charged-coupled device (CCD) as the detector. Raman spectra were excited on a Spectra-Physics model 127 He/Ne laser (633 nm) and recorded in the range of 400–1800 cm^{-1} and 2800–4000 cm^{-1}. Data manipulation, such as baseline adjustment, smoothing and normalising as well as interpretation, was performed using the Spectracalc software package GRAMS (Galactic Industries Corporation, NH, USA) and Microsoft EXCEL. Band component analysis was undertaken using the Jandel "Peakfit" software package which enabled the type of fitting function to be selected and allows specific parameters to be fixed or varied accordingly.

2.2.4. Electron microscopy

Scanning electron microscopy (SEM) images of the samples were taken on a JOEL JSM 35CF electron microscope at 15 kV at different magnifications. Electron micrographs of the samples were taken by the transmission electron microscopy method (TEM) at 80 kV with a JEOL JEX 1200X instrument.

3. Results and discussion

3.1. Powder X-ray diffraction (XRD)

The XRD patterns of the synthesis materials before and after various hydrothermal treatments are very similar. Identification of the crystalline components in the samples showed one major component, hydrotalcite $Mg_6Al_2(OH)_{16}(CO_3)\cdot 4H_2O$, accompanied by a trace amount of sodium nitrate, $NaNO_3$. The nitrate is persistently present even after thorough washing of the sample (Fig. 3). The (003) reflection is observed at ∼7.84 Å, corresponding to a hydrotalcite basal spacing of ∼23.5 Å. The XRD patterns obtained shows good agreement with the results obtained by Fernadez *et al.*, Kloprogge and Frost and by Thorez [5, 10, 12, 13].

The XRD patterns of all five samples undoubtedly demonstrate its layered structure. In the samples treated hydrothermally the (00*l*) reflections are more intense. A comparison of the patterns of the five samples, 1A, 1B, 2A, 2B and 2C shows that sample 2B is the most crystalline as it has the most intense and sharp peaks, followed by 1B, 2C, 1A and 2A respectively (Fig. 3). The relative intensity of the (003) reflection increases from the untreated sample, 2A, to the hydrothermally

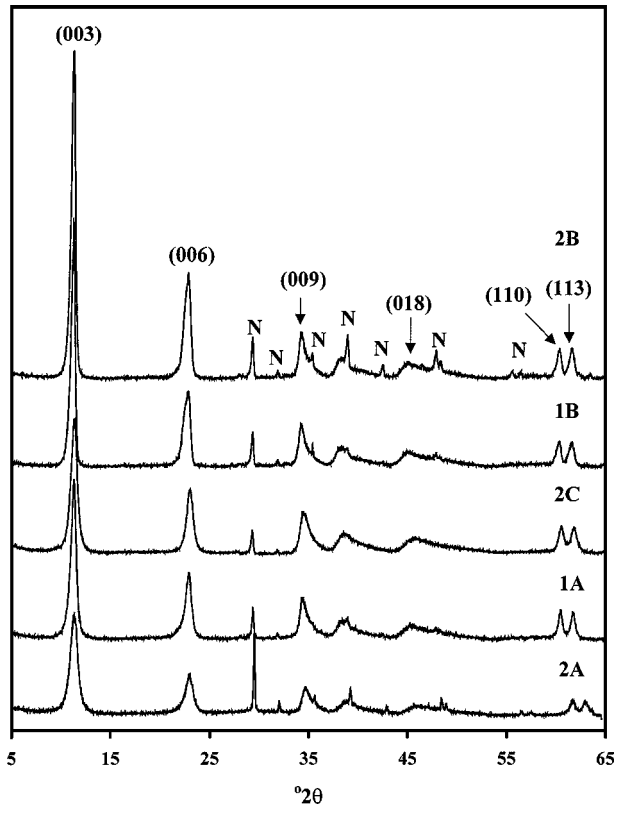

Figure 3 XRD pattern of the hydrothermally treated Mg-Al samples compared to the untreated sample: 2A–untreated, 1A, 2C, 1B, 2B. Where n represents the Na_2NO_3 peaks.

treated sample, 2B. Furthermore, the peak becomes sharper, where the width decreases from 2.2 °2θ for sample 2A to 0.5 °2θ in sample 2B. Thus 2B shows a larger crystallite size than 2A. For samples 1B, 2C and 1A the relative intensities, of the (003) reflection, are higher than for 2A but lower than for 2B. These samples are more crystalline than the untreated sample but less than sample 2B. Meaning that generally with aging crystallinity increases with increasing temperature and pressure. In addition, aging from a suspension in water appears to yield the most crystalline samples. Note, all samples shows signs, although in some cases minimal, of nitrate still being present, even after the second round of thorough washing.

The samples treated in the hydrothermal reactors were more crystalline than the water bath sample; this is due to the higher temperature and pressure reached in the bomb. Pressure also has a marked effect, such that sample 2C compared to sample 1A shows that crystallinity is increased when pressure is applied at the same temperature. When treated in water, instead of the mother liquid, a more highly crystallised compound was produced. This could be either due to the high pH or to the presence of soluble anions and cations. The presence of excess soluble ions, such as NO_3^{1-}, OH^- and Na^+, could hinder either the double layered structure from growing or the dissolution of smaller particles, so that the necessary ions are not available for the growth of other particles. Although the XRD patterns indicate that a nitrate species is present as a separate phase, there is a probability that some nitrate ions may be incorporated into the interlayer regions. With more

nitrate species present, for instance from the mother liquid, the probability of this occurring is greater. Thus treatment in water is preferable.

3.2. Thermal analysis

A representative TGA curve (sample 2B) is shown in Fig. 4 together with its derivative (DTG). The weight loss of the Mg/Al hydrotalcite starts at room temperature and is completed around 450°C. Three major weight losses are observed. The first step, ∼30–150°C, corresponds to loss of interparticle pore water, which is usually formed by condensation between particles [14]. This accounts for 14% of the initial weight of the sample. The second weight loss is almost completed by ∼235°C and corresponds to the loss of water molecules from the interlayer space, accounting for 18% of the initial weight of the sample. The third loss is completed by ∼430°C corresponding to 68% of the initial sample weight, and dehydroxylation of the hydroxide layers as well as loss of carbonate (interlayer anions), hence the inflection around 280°C. However, the gases evolved during thermal decomposition were not analysed, making it almost impossible to determine whether one loss corresponds the removal of carbonate or water. Theoretically the second peak should account for ∼12.9%, whilst the third peak corresponds to a loss ∼55.5%. The calculations were performed based on four molecules of water in the structural formulae $Mg_6Al_2(CO_3)(OH)_{16}{\cdot}4H_2O$. The DTA curve of the selected sample corresponds to the three major weight losses observed in the TG, with three major endothermic effects, where the maxima around ∼140, ∼225 and 310°C.

The loss of hydroxyl groups from the hydrotalcite layers is usually completed by 450°C [5, 14]. The hydrothermally treated samples all show a comparable thermal stability. Although hydrothermal treatment increases the crystallinity and crystallite size it has no recognisable effect on the thermal stability. Higher temperatures have been observed, ∼500°C, by Miyata [9], and have been described to be the result of increased layer charge density, which creates larger steric constraints on the interlayer species and larger hydrogen bonds [14]. Another reason why the final loss observed by Miyate [9] occurs at higher temperature is that the data has been recorded at a higher heating rate. Generally, a slow heating rate corresponds to overall lower temperatures for dehydration, dehydroxylation etc, due to the diminished diffusional effects [15].

3.3. Infrared spectroscopy

Several scientists have previously recorded the Mg/Al-hydrotalcite infrared spectrum [6, 9, 10, 16, 17]. The spectrum obtained for sample 2A (Fig. 5) shows a good agreement with these spectra with only slight variations in band positions. Table I shows the bands positions of all samples.

The very broad band centred around 3500 cm^{-1} is assigned to a complex of overlapping stretching modes of the hydroxyl groups present, both those in the brucite-type layer (Mg/Al-OH) and the interparticle and interlayer water molecules. The broadness of this peak is typically observed when hydroxyl bonds with a wide range of strengths exist [5]. Because of the lack of

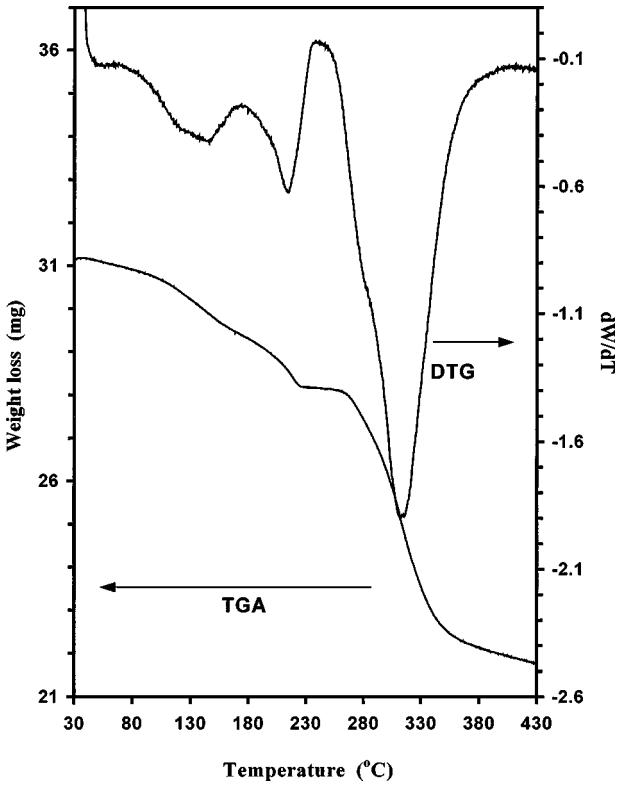

Figure 4 Thermal analysis of Mg/Al hydrotalcite of sample 2A (a) TGA (b) DTG.

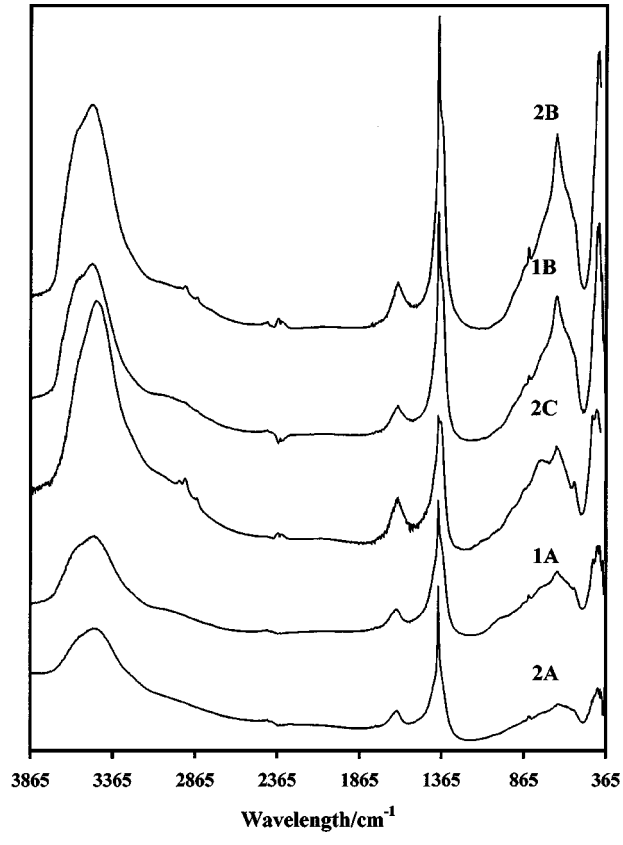

Figure 5 FT-IR spectra of samples 1A, 1B, 2A, 2B and 2C, in order of increasing crystallinity.

TABLE I Comparison of the infrared vibration of samples 1A, 1B, 2A, 2B and 2C, and there assignments

1A	1B	2A	2B	2C	Assignment
3200–3750	3000–3750	3300–3750	2800–3750	3300–3700	Hydroxyl stretching modes of free OH, water bonded water, Mg-OH, and Al-OH.
1642	1642	1642	1642	1639	H_2O deformation mode
1389	1384	1395	1387	1391	Asymmetric NO_3^{2-} stretch (ν_3)
1372	1361	1379	1364	1366	Asymmetric CO_3^{2-} stretch (ν_3)
835	836	844	843	872	Out of plane CO_3^{2-} bend (ν_2)
669	669	650	654	663	In plane CO_3^{2-} bend (ν_4)
553	565	553	565	551	M-O (Al-O) vibrational mode.
427	421	415	415	448	M-O (Mg-O) vibrational mode.

details of this band, band component analysis was not performed, which would have normally distinguished between the overlapping vibrational bands. However, work by Kloprogge *et al.* distinguished three bands at 2938, 3266 and 3471, corresponding to the CO_3-H_2O bridging mode, H-bonded interlayer water, and the 'M'-OH stretching mode, respectively [11]. One has to bear in mind that each OH in the hydrotalcite layer is linked to three cations; so OH-bonds are associated with either three of the same cations, or two of the same and one other cation. Hence the assignment 'M'-OH. The band at 1642 cm^{-1} is associated with the deformation mode of the water molecules (ν_2). Several bands below 1000 cm^{-1} are associated with the M-O vibrational modes (Mg-O, Al-O) in the brucite-type layer (Table I) [5]. The bands at 553 cm^{-1} and 415 cm^{-1} as well as a number of overlapping bands between 400–1000 cm^{-1} are also associated with Mg-O and Al-O vibrational modes. The peak at 415 cm^{-1} is assigned to Mg-O, while Al-O is assigned to the band at the higher frequency of 553 cm^{-1}, since Al has a higher mass number [17], taking into consideration that the bond lengths for Mg-O and Al-O are the same in the hydrotalcite.

The majority of the other bands observed in this spectrum are associated with the carbonate species present in the interlayer region. Assuming the carbonate species is present as the free ion (D_{3h}) and not specifically involved in any bonds, then only three bands will be present in the infrared spectrum [17, 18]. The ν_1 (A_1') carbonate (CO_3^{2-}) symmetric stretching mode is infrared inactive and only ν_2, ν_3 and ν_4 vibrations should be observed (Table II). The results of sample 2A are quite consistent with Farmers and Nakamotos' results [17, 18]. There are noticeable differences in the ν_2 and ν_4 as in this region of the infrared spectrum the peaks are very broad and are overlapped by the M-O vibrational modes.

The ν_3 antisymmetric stretching mode at ~1400 cm^{-1} is sharp at high intensity and broad at low intensity (Fig. 5). Hence, it was concluded that this peak was in fact composed of several bands superimposed on one another. Band component analysis of sample 2B, as it has the most defined band in this region (Fig. 6), shows clearly the presence of three overlapping bands: one sharp band and two broader bands. Although at slightly different frequencies then for the other samples, these bands can be assigned, in a similar way for all samples. The broader bands are assigned to the carbonate species. The logic behind this assignment is that carbonate in the free ion state is not bonded, or in a fixed

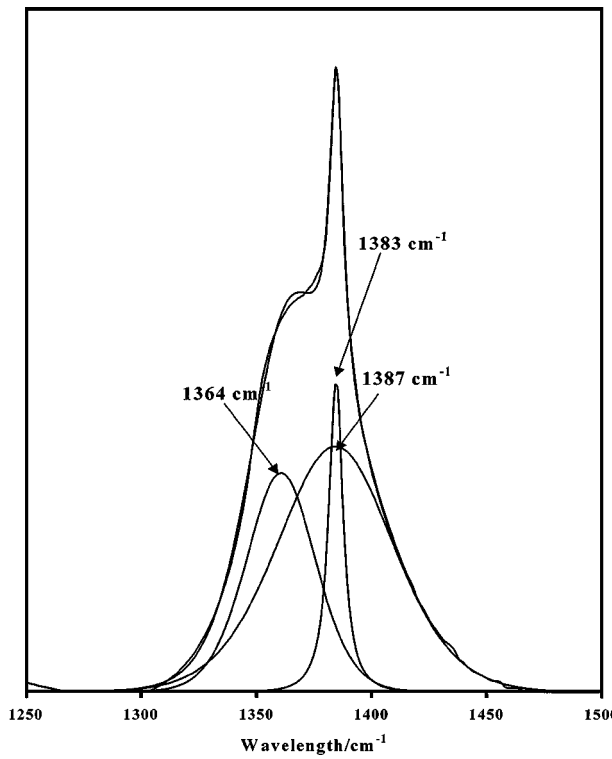

Figure 6 Band component analysis of Mg/Al hydrotalcite, sample 2B, of the asymmetric CO_3^{2-} stretch in the infrared spectrum.

TABLE II Vibrational modes of the carbonate free ion

Symmetry	Mode	Selection rule*	Nakamoto[17,18] (cm^{-1})	Sample 2A (cm^{-1})
A_1'	ν_1-symmetric stretch	R	1064	NO*
A_2''	ν_2-out of plane bend	IR	874	844
E'	ν_3-asymmetric stretch	IR/R	1415	~1400
E'	ν_4-in plane bend	IR/R	680	650

*R–Raman active, IR–Infrared active, NO–not observed in IR.

position, to any one particular molecule, instead its' charge is shared between the layered sheets. Thus carbonate bonds with a wide range of strengths would exist and results a broad peak. The sharper band is believed to be the result of the nitrate impurity, as crystalline nitrate always gives very sharp and intense bands. The nitrate antisymmetric stretching vibration, ν_3, is usually observed between 1410–1370 cm^{-1} [18, 19]. The nitrate ν_2 and ν_4 bands at 838 cm^{-1} and 727 cm^{-1}, respectively [19], occur very close to the carbonate vibrations and due to the broadness of the spectrum below 1000 cm^{-1} could not be distinguished. Although sodium nitrate appeared in the XRD as a separate phase, because the effects of high pH conditions the incorporation of nitrate ions incorporation into the hydrotalcite interlayer region along with the carbonate and water species can not be fully excluded.

The infrared spectrum can also be a useful tool to show the effect of hydrothermal treatment. As shown in Table I there are only slight variations in the band positions of the samples, which is expected since the structure does not change its short-range order. However, a comparison of the actual spectra (Fig. 5) shows quite a significant change with an increase in intensity of all bands. The bands below 1000 cm^{-1} become sharper. The spectra shows that hydrothermal treatment, results in an increase in intensity and decreases in bandwidth, regardless of the medium used. This is characteristic of an increase in order crystallinity. The degree of crystallinity within the treated samples differs from one to the other.

Sample 2A shows broader peaks than the aged samples meaning that it is less crystalline. The aged samples all have more intense and sharper peaks thus are more ordered than the untreated sample. The more ordered structure applies to not only the hydroxide layers, but also the interlayer space, thus giving rise to a more symmetric interaction between carbonate ions and water molecules, as also reported by Labajos *et al.* [3]. A comparison of the results of the infrared spectra of the treated samples shows good agreement with the XRD results, such that 2B is the most crystalline sample. Sample 2B shows the greatest increase in intensity and the sharpest bands. Sample 1B has less intense and sharp peaks than 2B but more than 2C, 1A and 2A. Sample 2C and 1A shows less intense and sharp peaks, respectively, than both 1B and 2B however more intense than 2A. So again, the hydrotalcite thermally treated in water gives better crystalline material than those treated in the mother liquid. Furthermore the infrared spectra shows that pressure affects the intensity of the bands.

3.4. Raman spectroscopy

The examination of the samples by Raman spectroscopy compliments the infrared study [20]. The most important regions of the Raman spectrum are between 1800–200 cm^{-1} and 4000–3000 cm^{-1}. The spectra of all samples are expected to show the same peaks except the treated samples are much sharper and intense (Fig. 7). For sample 2A the assignment of the bands observed have been worked out in more detail.

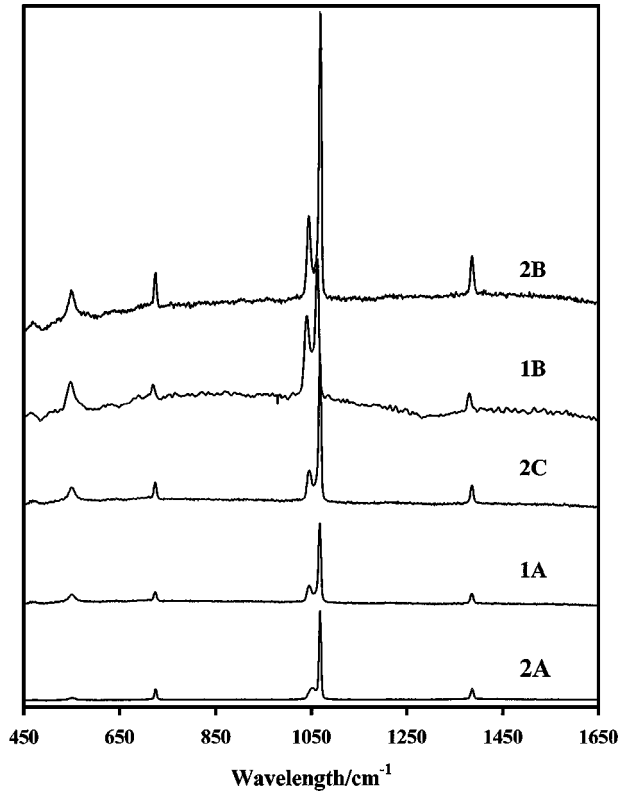

Figure 7 Raman spectra of samples 1A, 1B, 2A, 2B and 2C, in order of increasing crystallinity.

The weak band observed at 1671 cm^{-1}, which appeared much stronger in the infrared, is assigned to the deformation mode of water. The peak at 553 cm^{-1}, as well as other weak broad peaks below 1000 cm^{-1}, are assigned to various M-O vibrations, similar to those observed in the infrared spectrum. Table II shows the expected values of the three Raman active modes of carbonate [17–19]. Table III reports the observed bands of the hydrotalcites and their assignments. The band at 726 cm^{-1} is the in-plane bending mode (ν_4), at 1062 cm^{-1} is the symmetric stretching mode (ν_1) and at 1390 cm^{-1} is the antisymmetric stretching mode of the carbonate group. As expected, based on the infrared observations, there is an extra peak around 1068 cm^{-1}, which is assigned to the nitrate symmetric stretching mode (ν_1, A_1'). This peak is more resolved than in the infrared spectrum and a similar band has been observed at 1068 cm^{-1} for $NaNO_3$ by Ross [19]. The nitrate was assigned to the sharper and more intense peak, as carbonate was expected to be somewhat broad. The ν_3 and ν_4 modes of nitrate are also present, but

TABLE III Band assignment of the Raman active vibrational modes of the four samples

1A	1B	2A	2B	2C	Band Assignment
1671	1669	1670	1675	1671	Water deformation mode
1385	1382	1390	1390	1388	Asymmetric carbonate stretch, ν_3.
1068	1069	1068	1071	1069	Symmetric nitrate stretch, ν_1
1061	1055	1062	1063	1064	Symmetric carbonate stretch, ν_1
727	726	726	726	724	In plane bend of carbonate, ν_4
550	553	553	550	551	M-O vibrations
469	468	471	471	466	M-O vibrations

are not separately observed because they are superimposed on the much stronger ν_3 and ν_4 modes of the carbonate.

A comparison of the five samples spectra, (Fig. 7, Table III), shows that although the band positions are similar the intensities are quite different. This figure shows that the relative intensities increase from sample 2A, 1A, 2C, 1B and 2B, respectively. Furthermore the sharpness of the bands also increase from sample 2A to 2B in the same order, such that sample 2B has not only the most intense but also the sharpest bands. Several peaks in the lower frequency region becomes more obvious, peaks which weren't visible in the spectrum of 2A. The results of the Raman spectra are consistent with the infrared and XRD results, as it shows that sample 2B is the most crystalline, followed by 1B, 2C, 1A and 2A.

The hydroxyl-stretching region of the spectra, in the region of 3000–4000 cm^{-1}, shows a broad hydroxyl band, in which a number of overlapping peaks can be distinguished. Band component analysis of sample 2A (Fig. 8) confirms that a number of bands contribute to the broad peak. These bands are due to the CO_3-H_2O bridging mode, H-bonded interlayer water, and the 'M'-OH stretching modes, where the peak at 3687 cm^{-1} is typical of an 'Al'-OH stretch. The other bands are assigned to the interlayer water, free water, and other hydroxyl stretches, among which included 'Mg'-OH at a lower frequency than the 'Al'-OH stretch as it is lower in molecular weight, remembering that every OH is connected to three cations.

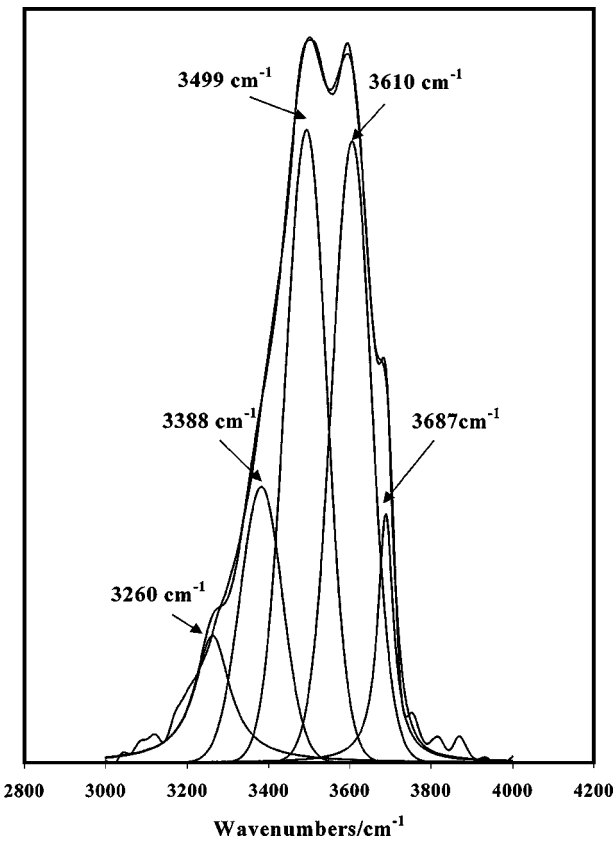

Figure 8 Band component analysis of Mg/Al hydrotalcite sample 2A, of the Hydroxyl region, in the Raman spectra.

3.5. Electron microscopy

The development of electron microscopy has permitted the precise determination of the of the hydrotalcite particles. Furthermore, it demonstrates the range of particles sizes [21]. Essentially SEM images provide a morphological and textural description of the sample of interest. Fig. 9 shows the morphology of the two extremes: hydrotalcite sample 2A and the highly crystalline sample 2B. Although crystallinity is not necessarily coupled to crystal size, in most cases it is observed to be true. Sample 2A has a smaller particle size compared to sample 2B, which is in agreement with the XRD, infrared and Raman observations. Furthermore, sample 2A (Fig. 9) reveals a more fibrous morphology with small flakes commonly grouped together in irregular aggregates, whereas sample 2B (Fig. 9) shows a more layered structure. Actual particle sizes can be better determined from TEM images.

TEM images of the samples 1A, 1B, 2A, 2B and 2C show an increase in both crystallinity and crystallite size upon aging. (Fig. 10). Sample 2A, the untreated sample, contains aggregates of very small thin platelets of approximately 1nm in diameter (Fig. 10). These particles have an irregular structure and don't appear to be hexagonal in shape. Sample 2B, the highest crystalline sample, has definite hexagonal plate shaped particles (Fig. 10), with a well-defined electron diffraction

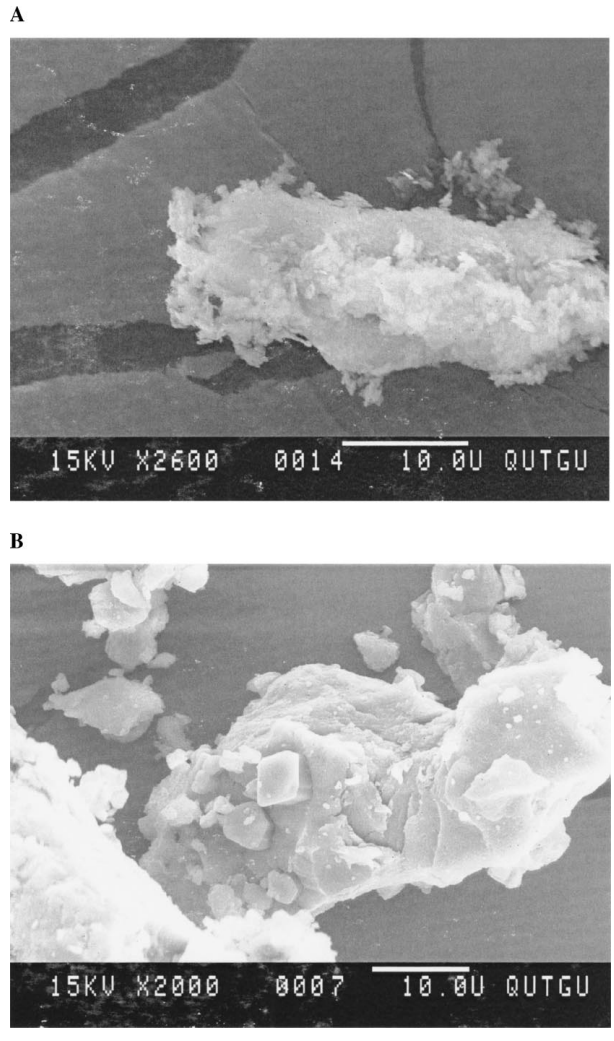

Figure 9 SEM images of hydrotalcite samples; (a) 2A, (b) 2B.

(a)

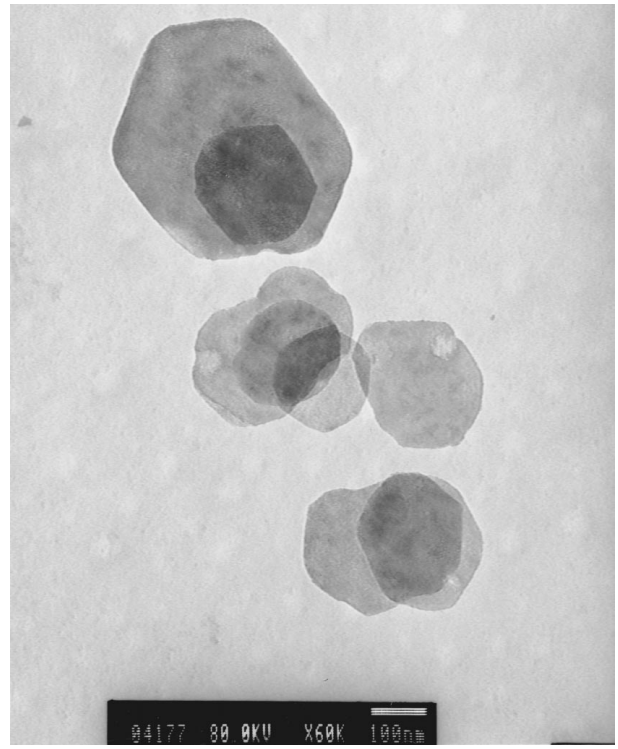

(b)

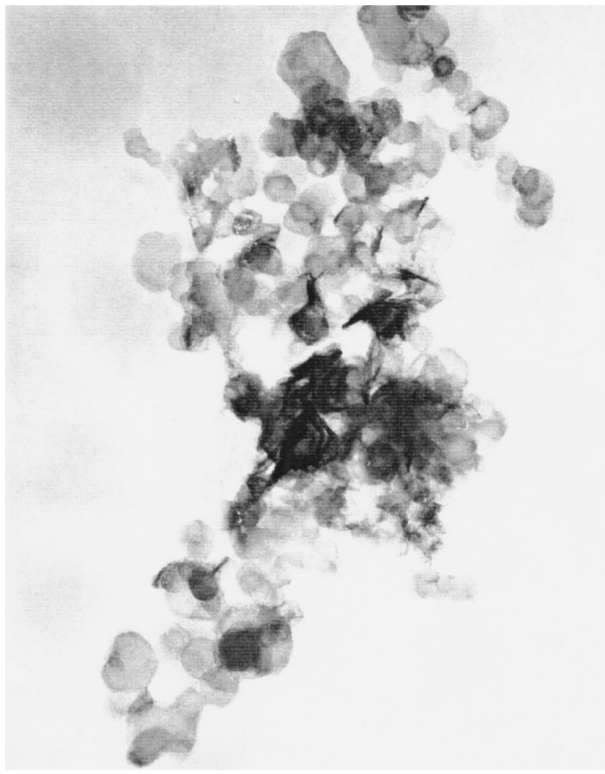

(c)

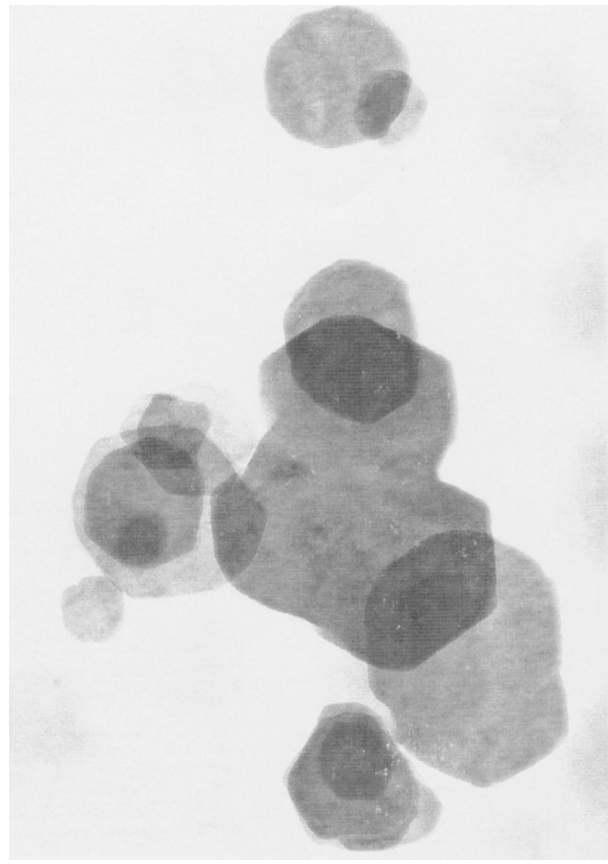

(d)

Figure 10 TEM images of hydrotalcite samples; (a) 2A, (b) 2B, (c) 1A, and (d) 1B.

pattern [14]. These particles are considerably larger, ~300 nm, than those of sample 2A and are regular throughout the sample. This means that with aging predominant growth occurs on the edges resulting in relatively thin, hexagonal plate shaped crystals [2, 22]. In addition some stacking does occur upon aging as evidenced by the decrease in peak width of the (00*l*) reflections in the XRD. The hexagonal shaped particles of this sample provided further evidence that the sample 2B is a more crystalline sample than sample 2A.

Thus aging increases crystallinity and allows time for the classical hexagonal shape of the hydrotalcite to form. Throughout this sample there are a limited number of smaller particles, the reason for this is that with aging the smaller particles get smaller and bigger particles grow, due to dissolution, until no smaller particles remain, a process commonly known as Ostwald ripening. This effect would be noticed even stronger with prolonged aging.

These two extremes demonstrate the diversity of the sample structure from highly crystalline sample to not so crystalline sample. Sample 1B looks very similar to sample 2B with the hexagonal shaped crystals, 250–300 nm, with well-developed diffraction patterns. The actual crystals are smaller than the sample 2B. Sample 2C shows very fine and feathery like particles. These particles are very small and crystals are not well defined. Further more no hexagonal shape particles exist, however the particles are flat and stacked. The average particle size of this sample is ∼40 nm, considerably less than 2B and 1B. Sample 1A is rather different such that the crystals still show very well developed electron diffraction patterns, indicating high crystallinity. However, the hexagonal shape is absent and the crystals are very thin and flaky. Confirming that sample 1A is the least crystalline sample of the treated samples, with a smaller particle size of ∼20 nm.

4. Conclusion

XRD, infrared and Raman spectroscopy, electron microscopy and thermal analysis are powerful methods employed in the characterisation of hydrotalcites. The effect of hydrothermal treatment on hydrotalcites showed a definite increase in crystallinity in all samples, where the degree of crystallinity depended on the media of treatment. It was observed that the samples treated in thermal bombs at autogenous pressure and at 150°C, exhibited the largest increase in crystallinity and crystal size, due to the higher temperature reached, in combination with the increased pressure. A comparison of the sample treated with temperature as compared to one treated with temperature and pressure showed an increase in crystallinity and particle size. In addition, hydrotalcite aged in water obtained a higher degree of crystallinity than those aged in the mother liquid. The high pH and the presence of soluble ions may hinder the dissolution of small particles and subsequent growth of larger particles.

Acknowledgements

The authors thank Tony Raftery for assistance with X-ray diffraction. Loc Duong and Thor Bostrom, of the Analytical Electron Microscopy Facility at QUT, are thanked for their assistance with the SEM and TEM. The contribution of Shane Russell with the DTA/TGA is greatly appreciated. The financial and infrastructural support of the QUT, Centre for Instrumental and Developmental Chemistry, is gratefully acknowledged.

References

1. A. VACCARI, *Catal. Today* **41** (1998) 53.
2. W. T. REICHLE, *Solid State Ionics* **22** (1986) 135.
3. F. M. LABAJOS, V. RIVES and M. A. ULIBARRI, *J. Mater. Sci.* **27** (1992) 1546.
4. W. T. REICHLE, *Chemtech.* (1986) 58.
5. J. M. FERNANDEZ, M. A. ULIBARRI, F. LABAJOS and V. RIVES, *J. Mater. Chem.* **8** (1998) 2507.
6. S. MIYATA, *Clays and Clay Minerals*. **23** (1975) 369.
7. M. BELLOTTO, B. REBOURS, O. CLAUSE, J. LYNCH, D. BAZIN and E. ELKAIM, *J. Phys. Chem.* **100** (1996) 8527.
8. R. M. BARRER. "Hydrothermal Chemistry of Zeolites" (Academic Press, London, 1982) ch. 4, p. 96.
9. S. MIYATA, *Clays and Clay Miner.* **28** (1980) 50.
10. J. T. KLOPROGGE and R. L. FROST, *Phys. Chem. Chem. Phys.* **1** (1999) 1641.
11. J. T. KLOPROGGE, R. L. FROST and L. HICKEY, *Clays Clay Miner*. accepted with revisions (1999).
12. J. T. KLOPROGGE and R. L. FROST, *J. Solid State Chem*. accepted with revisions (1999).
13. J. THOREZ, "Practical Identification of Clay Minerals: a Handbook for Teachers and Students in Clay Mineralogy" (Belgium State University Press, Dison: Lelotte, 1976).
14. S. K. YUN and T. J. PINNAVAIA, *Chem. Mater.* **7** (1995) 348.
15. J. T. KLOPROGGE, J. B. H. JANSEN and J. W. GEUS, *Clays Clay Miner*. **38** (1990) 409.
16. J. A. GADSDEN, "Infrared Spectra of Minerals and Related Inorganic Compounds" (Butterworths, England, 1975) p. 75.
17. V. FARMER, "The Infrared Spectra of Minerals" (Mineralogical Society, England, 1974).
18. K. NAKAMOTO, "Infrared and Raman Spectra of Inorganic and Coordination Compounds" (John Wiley & Sons, USA, 1997) p. 84.
19. S. D. ROSS, "Inorganic Infrared and Raman Spectra" (McGraw-Hill Book Company, London, 1972) p. 140.
20. Bernhard Schrader, "Infrared and Raman Spectroscopy: Methods and Applications" (Weinheim, New York, VCH, 1995).
21. R. E. GRIM, "Clay Mineralogy," 2nd ed. (McGraw-Hill, USA, 1968).
22. W. T. REICHLE, S. Y. KANG and D. S. EVERHARDT, *J. Catal.* **101** (1986) 352.

Received 19 July 1999
and accepted 8 February 2000